Motion Compensation in Bistatic Airborne SAR Based on a Geometrical Approach

Amaya Medrano Ortiz, Holger Nies, Otmar Loffeld
Center for Sensorsystems (ZESS)
University of Siegen
Paul-Bonatz-Str. 9-11
D-57068 Siegen
Germany

medrano-ortiz@ipp.zess.uni-siegen.de

ABSTRACT

Common efficient SAR processing algorithms, e.g. Chirp Scaling (CS) and Omega-K are based on nominal operational conditions, that is, rectilinear flight trajectory and constant airborne attitude and forward velocity. Unfortunately, due to atmospheric turbulences and manoeuvring errors, these conditions are often violated in real SAR systems. Airborne sensors, in contrary to spaceborne sensors, always show deviations from the ideal flight track. SAR imaging from such unstable platform requires an accurate measurement of the antenna position during the flight and a modified processing scheme, which takes into account the non-linear movement of the sensor.

Hence, a crucial problem in most airborne SAR sensors is the compensation of motion errors (i.e. the compensation of changes of the platform velocity vector in orientation and/or in magnitude). If not corrected, the image quality will considerably degrade.

Experiments with different sets of bistatic airborne SAR data are performed based on a geometrical solution, and some very promising results are presented in this paper.

1.0 INTRODUCTION

While performing data acquisitions, airborne sensors are very sensitive to the effects of unstable weather conditions. The main effects observed are the loss of geometric resolution and radiometric accuracy, reduction of image contrast, azimuth ambiguities and strong phase distortions. As modern SAR systems are continuously developing into the direction of higher spatial resolution, processing algorithms are required which are able to deal with high bandwidths combined with long azimuthal integration intervals, even in presence of motion errors.

The use of motion compensation to achieve airborne SAR focusing has been studied for a long time. Ideal compensation requires precise knowledge of the relative geometry between the radar and each illuminated target for every transmitted pulse.

While motion compensation in monostatic SAR systems is relatively straight forward and very mature, the situation in bistatic SAR imaging is slightly more complex: In place of one monostatic motion trajectory we must consider the individual trajectories of transmitter and receiver, in place of one monostatic look direction depending on slant range and momentary Doppler frequency we need to consider the look directions of transmitter and receiver.

Ortiz, A.M.; Nies, H.; Loffeld, O. (2006) Motion Compensation in Bistatic Airborne SAR Based on a Geometrical Approach. In *Bistatic-Multistatic Radar and Sonar Systems* (pp. 19-1 – 19-10). Meeting Proceedings RTO-MP-SET-095, Paper 19. Neuilly-sur-Seine, France: RTO. Available from: http://www.rto.nato.int/abstracts.asp.

In this work we present a geometrical approach for motion compensation derived from a flat flight trajectory, which will be gained through minimization of the quadratic errors. The position in SAR terms can be expressed by means of: offset of the Doppler spectrum, errors during motion time, phase errors and sampling errors in azimuth direction. The errors during motion time and the false sampling in azimuth direction due to the small variation of velocities of the platforms and high sampling frequency will not be considered in this paper.

2.0 GEOMETRY OF THE PROBLEM

For each sample in the time domain, the exact position for SAR data can be given by means of the offset of the Doppler spectrum and phase errors. Thus, the position for the point target, the transmitter and the receiver for each time instant can be simulated, and defined with vectors:

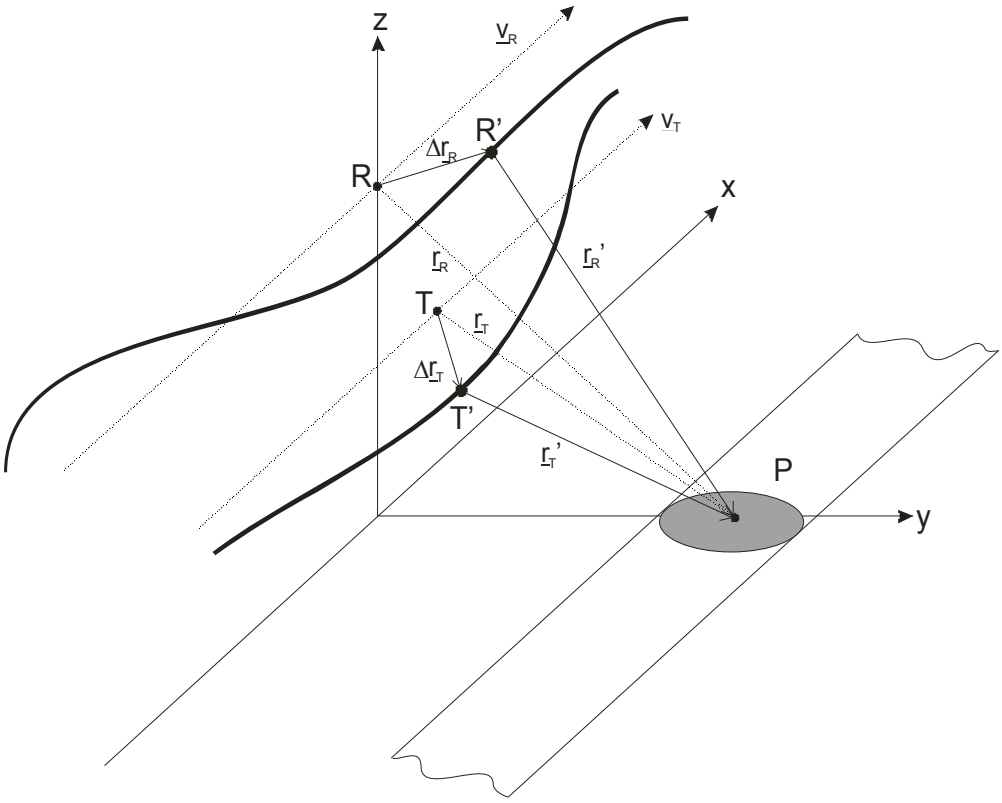

Figure 1: Idealized and corrected trajectories

In bistatic SAR, the range to a point target can be expressed as the superposition of transmitter and receiver ranges:

$$r = r_R + r_T = \underline{e}_R \cdot \underline{r}_R + \underline{e}_T \cdot \underline{r}_T \tag{1}$$

where $\underline{e}_R$, $\underline{e}_T$ are the line of sight vectors of receiver and transmitter, $\underline{r}_R$, $\underline{r}_T$ the corresponding slant range vectors.

The overall slant range can be replaced by nominal slant range plus motion errors, which can be determined using Kalman filter estimates of true position and velocities of the carrier platforms in relation to some nominally wanted reference trajectories:

$$r(t)+\Delta r(t)= \underline{e}_R(t)\cdot\left(\underline{r}_R(t)+\Delta\underline{r}_R(t)\right) + \underline{e}_T(t)\cdot\left(\underline{r}_T(t)+\Delta\underline{r}_T(t)\right) \tag{2}$$

From this expression, we can extract the difference between nominal and corrected values of the position:

$$\Delta r(t)=\underline{e}_R(t)\cdot\Delta\underline{r}_R(t)+\underline{e}_T(t)\cdot\Delta\underline{r}_T(t) \tag{3}$$

3.0 CONSIDERATIONS PREVIOUS TO THE MOTION COMPENSATION

3.1 Improvement of the position and trajectory estimates

The first step to consider for the motion compensation is the improvement of the noisy position and velocity measurements. The observation noise can be cancelled, since the airplanes move independently from each other, yielding different motion error contributions. Thus, the estimates of the position and trajectory can be considerably improved by using two individual Kalman filters. These optimized estimates will be necessary in order to obtain the ideal tracks of transmitter and receiver.

In fact, by means of using the Kalman filter for the GPS/INS integration, an excellent interpolated data set of the trajectories of transmitter and receiver for each time instant (same as PRF) is obtained. Section 4 will explain the use of these ideal tracks for the motion compensation.

3.2 Simplification of the bistatic processing

Generally the bistatic processing problem is not completely solved, though there are some promising approaches. The problem is the increasing complexity, coming up with increasing amount of time variant parameters. Two important parameters use our bistatic processing approach, which are giving the bistatic grade of the configuration:

$$a_0=\tau_{0T}-\tau_{0R} \tag{4}$$

$$a_2=\frac{R_{0T}}{R_{0R}} \tag{5}$$

a_0 is the difference between azimuth times of closest approach of the transmitter and the receiver, and a_2 is the ratio of the minimal slant ranges at the point of closest approach. Since the trajectories in this special case are considered straight and parallel, we can simplify these bistatic parameters: a_0 will have a constant variation due to the different velocities of the transmitter and the receiver. a_2 will be constant over time.

Further details of the bistatic processing algorithm developed by our SAR group in ZESS can be found in [3].

3.3 Calculation of the centroid's position

In monostatic processing, the centroid can be easily calculated by means of the squint and look angle. Nevertheless, in the bistatic case the situation changes, since we have two different velocities, squint and look angles. Thus, we need to analyze the overlapping swaths of transmitter and receiver.

Since now we have two different velocities in terms of magnitude and direction, the distance between both semi-monostatic centroids of transmitter and receiver will change over time. Thus, we need to determine the position of the common centroid in order to proceed with the motion compensation.

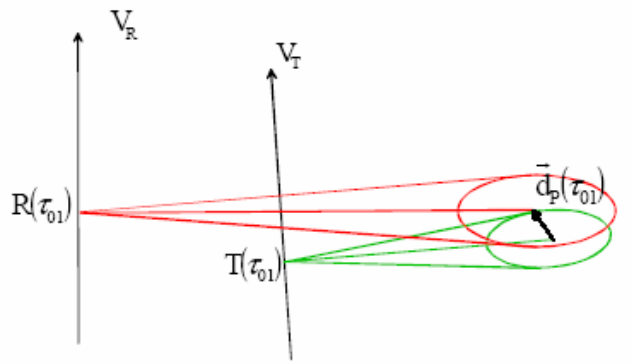

Figure 2: Overlapping swaths of transmitter and receiver in bistatic geometry

The first step is obtaining the combined and normalized intensity distribution, $I(r_{rn}, r_{az})$, which can be calculated by multiplying the individual intensity distributions on flat ground of the antennas of transmitter and receiver:

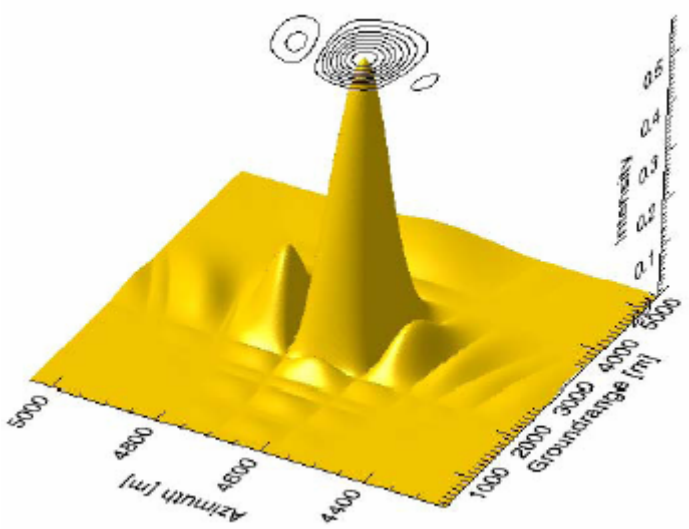

Figure 3: Distribution of the combined bistatic antenna intensity

From Figure 3, we can observe that the distribution includes a bistatic deformation, if we compare with a monostatic distribution. Because of this asymmetry, the centroid will not necessarily coincide with the maximum of this distribution. As direct consequence of this, we will need to calculate the mean values for range and azimuth direction:

$$\mu_{rn} = \int_{-\infty}^{\infty} r_{rn} \cdot \left(\int_{-\infty}^{\infty} I\left(r_{rn}, r_{az}\right) \cdot dr_{az} \right) \cdot dr_{rn} \tag{6}$$

$I(r_{rn}, r_{az})$ is the normalized intensity, normalized to unit area.

$$\mu_{az} = \int_{-\infty}^{\infty} r_{az} \cdot \left(\int_{-\infty}^{\infty} I\left(r_{rn}, r_{az}\right) \cdot dr_{rn} \right) \cdot dr_{az} \tag{7}$$

μ_{rn} represents the mean in range direction and μ_{az} the mean in azimuth direction.

4.0 IDENTIFICATION OF THE ERRORS FOR MOTION COMPENSATION

4.1 Modelling the phase errors

The phase error can be defined directly from the real and faulty distance values showed in (3), as follows:

$$\varphi_{err}(t) = \frac{2\pi}{\lambda} \cdot \left(r'(t) - r(t) \right) = \frac{2\pi}{\lambda} \cdot \Delta r(t) \tag{8}$$

4.2 Modelling the offset of the Doppler spectrum

This approach assumes that the derivative of the pointing vectors, $\underline{e}_R, \underline{e}_T$, nearly goes to zero:

$$\begin{aligned} r_R &= \underline{e}_R \cdot \underline{r}_R \\ r_T &= \underline{e}_T \cdot \underline{r}_T \end{aligned} \Rightarrow \begin{aligned} \dot{r}_R &= \underline{e}_R \cdot \underline{v}_R \\ \dot{r}_T &= \underline{e}_T \cdot \underline{v}_T \end{aligned} \tag{9}$$

From the geometry, and considering (9), we can express the Doppler centroid frequency and the error term as:

$$f_D = \frac{1}{2\pi} \cdot \left(\frac{2\pi}{\lambda} \cdot \dot{r}_R + \frac{2\pi}{\lambda} \cdot \dot{r}_T \right) = \frac{\underline{e}_R \cdot \underline{v}_R}{\lambda} + \frac{\underline{e}_T \cdot \underline{v}_T}{\lambda} \tag{10}$$

$$\Delta f_D = \frac{1}{2\pi} \cdot \left(\frac{2\pi}{\lambda} \cdot \Delta\dot{r}_R + \frac{2\pi}{\lambda} \cdot \Delta\dot{r}_T \right) = \frac{\underline{e}_R \cdot \Delta\underline{v}_R}{\lambda} + \frac{\underline{e}_T \cdot \Delta\underline{v}_T}{\lambda} \tag{11}$$

On the other hand, the offset of the Doppler spectrum is obtained with the determination of the difference of the Doppler frequency of the real trajectory with the ideal:

$$\Delta f_D = f_D - f'_D \tag{12}$$

Also in this case, GPS measuring and Kalman filtering is considered.

5.0 ERROR COMPENSATION

The corrections of the phase errors of a target (near, centred and far range) can be calculated for each time instant through a compensation term for each range line, since the variation of the phase error in range is approximately linear:

$$g_{rn_{corr}}(t) = g'_{rn}(t) \cdot e^{-j\varphi_{err}(t)} \tag{13}$$

In an analogous way, for compensating the offset of the Doppler spectrum, the azimuth lines are multiplied on time domain with the corresponding correction term:

$$g_{az_{corr}}(t) = g'_{az}(t) \cdot e^{-j2\pi\Delta f_D t} \tag{14}$$

6.0 EXPERIMENTS

6.1 The parameters

To verify the suitability of our approach, we performed an analysis of a set of bistatic airborne SAR data delivered by FGAN/FHR's PAMIR/AER-II systems (http:/www.fhr.fgan.de/fhr/fhr_home_e.html).In this set AER-II was used as transmitter, while PAMIR was used as receiver. The parameters are shown in Table 1:

Parameter	Value
Velocity of the transmitter ($\mathbf{v_T}$)	101 m/s
Velocity of the receiver ($\mathbf{v_R}$)	97 m/s
Distance transmitter-point target at the point of closest approach ($\mathbf{R_{0T}}$)	3057 m
Distance receiver-point target at the point of closest approach ($\mathbf{R_{0R}}$)	3835 m
Doppler frequency ($\mathbf{f_{DC}}$)	21.2 Hz
Bistatic parameter ($\mathbf{a_0}$)	1.298 s
Bistatic parameter ($\mathbf{a_2}$)	0.7972

Table 1: Parameters of the experiment

6.2 First tests

Before applying our approach on the whole set of data, we generated raw data of a single point target using the original trajectories of transmitter and receiver during the flight campaign. We can find the azimuth time of closest approach of transmitter and receiver with respect to the point target within the time window that will be showed in Figure 6 and Figure 7. This test leads us to the following graphical result for the processing without motion compensation:

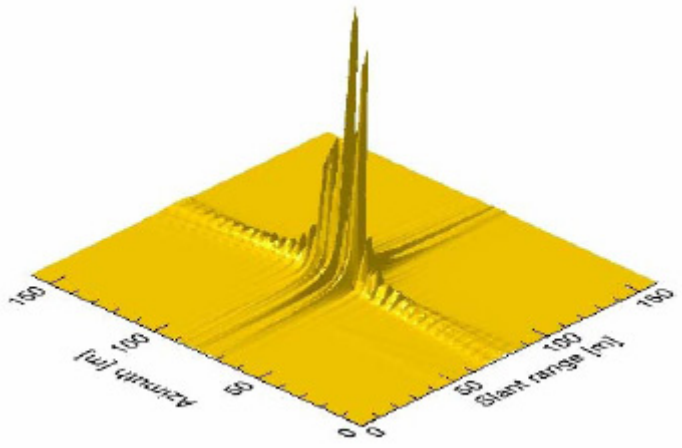

Figure 4: Simulated raw data after processing without motion compensation

After applying the proposed motion compensation approach, the result considerably improves:

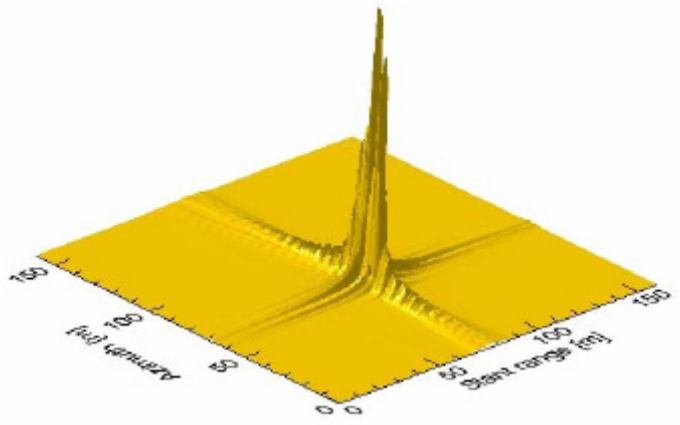

Figure 5: Simulated raw data after processing with motion compensation

Figure 4 shows the reconstruction of the point target, which is correct in range direction but defocused in azimuth direction. After using our approach, we can see on Figure 5 that the result is considerably improved. This leads us to a positive conclusion about the viability of using this geometrical approach for motion compensation with the raw data provided by the PAMIR/AER-II systems.

However, we can also see in Figure 5 that the image is not completely focused. This is due to the assumption of having parallel trajectories of the platforms and thus, using a simplified SAR processing algorithm based on a monostatic kernel convoluted with a bistatic deformation term.

6.3 Final experiments

After verifying the results of a single point target, our geometrical approach was applied to the whole set of raw data. As first step, we calculate the corresponding phase error and the error caused by the offset of the Doppler spectrum, as explained in Section 4. The phase error for different range distances results on the following:

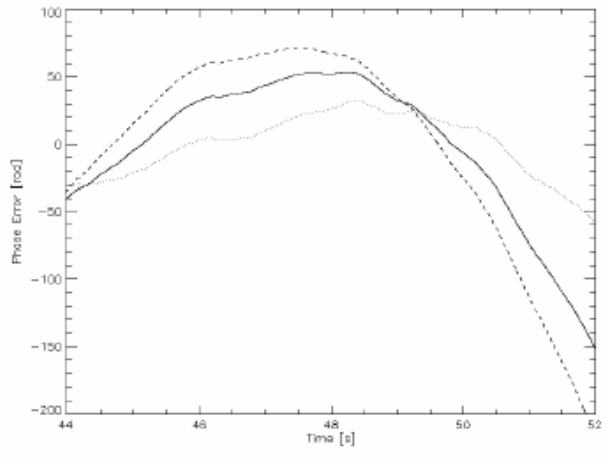

Figure 6: Cut-out of the phase error (dotted line: near range, solid line: scene center, dashed line: far range)

And the representation of the real and faulty Doppler frequency:

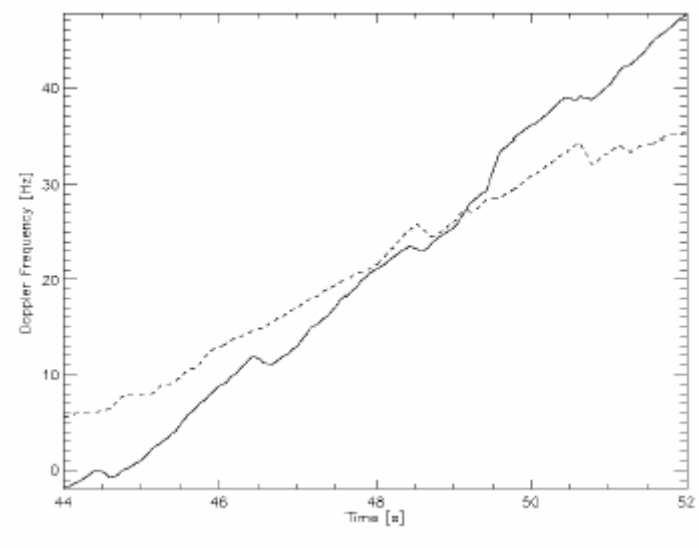

Figure 7: Cut-out of the Doppler frequency over time (solid line: real frequency, dashed line: erroneous frequency)

Once the compensation terms for phase and Doppler spectrum were calculated, the motion compensation was carried out. The following figure represents the reconstructed scene without any motion compensation:

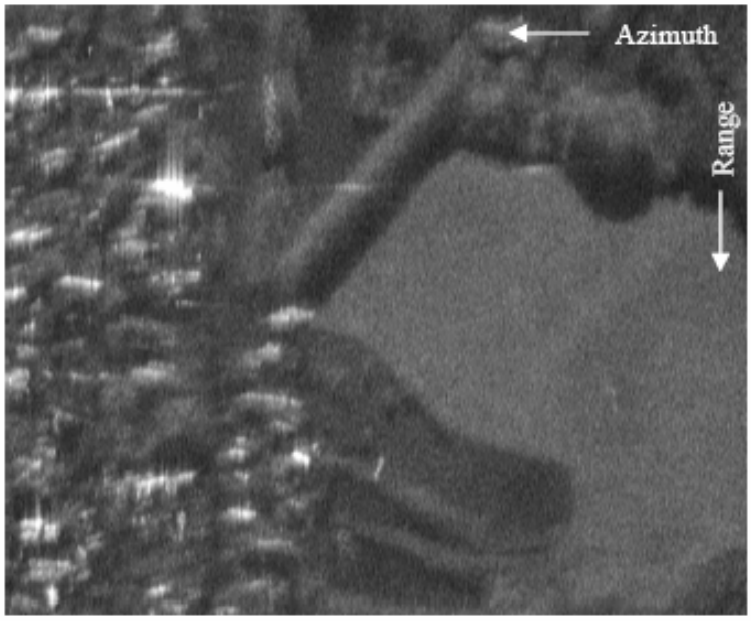

Figure 8: Resulting scene after processing without motion compensation (cut-out)

And analogously, the reconstructed scene after processing with our geometrical approach for motion compensation:

Figure 9: Resulting scene after processing with motion compensation (cut-out)

We can appreciate that, while Figure 8 shows a camera shake effect on the image, the cut-out represented on Figure 9 seems to be better focused. But analogously to Figure 5, we cannot see a perfectly focused image, due to the initial assumption of parallel trajectories of transmitter and receiver.

7.0 CONCLUSIONS

In this paper, a geometrical approach was proposed for a first order motion compensation. It is implicitly clear that in order to yield a better result, it is strictly necessary to improve the estimates of the position and trajectory of the carrier platforms of transmitter and receiver by means of Kalman filtering. A common centroid's position is calculated taking into account the overlapping swaths of transmitter and receiver in bistatic geometry. Once these prerequisites were satisfied, determining the error compensation terms was a relatively easy task.

Indeed, we could see from the graphical result of the experiments that our approach improves the result of the bistatic processing. However, it is also clear that a second order motion compensation is still needed in order to obtain an optimally focused image. Further research will take into account this issue.

8.0 AKNOWLEDGMENTS

The authors would kindly like to thank Prof. Dr. J. Ender, Dr. A. Brenner and I. Walterscheid from FGAN's Institute for High Frequency Physics and Radar Techniques (FHR, Watchberg, Germany) for the good cooperation, also for providing the raw data and technical documents. We would also gratefully like to acknowledge the support of DAAD's IPP Programme and the funding of the Ministry of Science of Nordrhine Westfalia.

9.0 REFERENCES

[1] H. Nies, O. Loffeld, K. Natroshvili, A. Medrano, J. H. G. Ender, “A Solution for Bistatic Motion Compensation”, submitted for IGARSS 2006, Denver, USA.

[2] H. Nies, “Zentrale und Dezentrale Estimationsverfahren in Multi-Sensorsystemen und deren Anwendung am Beispiel hochgenauer Positionsbestimmung”, PhD Thesis, University of Siegen, 2006.

[3] O. Loffeld, H. Nies, V. Peters and S. Knedlik, “Models and Useful Relations for Bistatic SAR Processing”, IEEE Transactions on Geoscience and Remote Sensing, Vol. 42, No. 10, October 2004.

[4] H. Nies, O. Loffeld, K. Natroshvili, I. Walterscheid, A. R. Brenner, „Parameter Estimation for Bistatic Constellations“, Proceedings of the IGARSS 2005, Seoul, Korea.

[5] H. Nies, O. Loffeld, K. Natroshvili, „Analysis and Focusing of Bistatic Airborne SAR Data“, Proceedings of the EUSAR 2006, Dresden, Germany.